International Journal of Pharmaceutics 402 (2010) 221–230

Contents lists available at ScienceDirect

International Journal of Pharmaceutics

journal homepage: www.elsevier.com/locate/ijpharm

Pharmaceutical Nanotechnology

Silicalites and Mesoporous Silica Nanoparticles for photodynamic therapy

Ouahiba Hocine[a], Magali Gary-Bobo[d,e,f,g,1], David Brevet[a], Marie Maynadier[d,e,f,g], Simon Fontanel[d,e,f,g], Laurence Raehm[a,*], Sébastien Richeter[a], Bernard Loock[h,i], Pierre Couleaud[j], Céline Frochot[j], Clarence Charnay[b], Gaëlle Derrien[b], Monique Smaïhi[c], Amar Sahmoune[l], Alain Morère[k,**], Philippe Maillard[h,i,***], Marcel Garcia[d,e,f,g], Jean-Olivier Durand[a]

[a] Equipe Chimie Moléculaire et Organisation du Solide, Institut Charles Gerhardt Montpellier, UMR 5253 CNRS-UM2-ENSCM-UM1, CC1701 Place Eugène Bataillon, 34095 Montpellier Cedex 05, France
[b] Equipe AIME, Institut Charles Gerhardt Montpellier, UMR 5253 CNRS-UM2-ENSCM-UM1, CC1701 Place Eugène Bataillon, 34095 Montpellier Cedex 05, France
[c] Institut Européen des Membranes, UMR 5635 CNRS-UM2, 1919, route de Mende, 34293 Montpellier cedex 05, France
[d] IRCM, Institut de Recherche en Cancérologie de Montpellier, Montpellier F-34298, France
[e] INSERM, Unité 896, Montpellier F-34298, France
[f] Université Montpellier1, Montpellier F-34298, France
[g] CRLC Val d'Aurelle Paul Lamarque, Montpellier F-34298, France
[h] UMR 176 CNRS/Institut Curie, Institut Curie, Bât 110-112, Université Paris-Sud, F-91405 Orsay, France
[i] Institut Curie, Section de Recherches, Centre Universitaire, Université Paris-Sud, F-91405 Orsay, France
[j] Laboratoire Réactions et Génie des Procédés, UPR 3349, Nancy-University, 1, rue Grandville BP 20451, 54001 Nancy Cedex, France
[k] UMR 5247 CNRS- UM 2 et UM1 - Institut des Biomolécules Max Mousseron, Ecole Nationale Supérieure de Chimie de Montpellier, 8 rue de l'Ecole Normale, 34296 Montpellier, France
[l] Université Mouloud Mammeri de Tizi-Ouzou, Route de Hasnaoua BP 17 RP 15000, Tizi-Ouzou, Algeria

ARTICLE INFO

Article history:
Received 28 June 2010
Received in revised form
30 September 2010
Accepted 1 October 2010
Available online 8 October 2010

Keywords:
Nanoparticles
Mesoporous
Organized porosity
Silica
PDT
Targeting
Mannose

ABSTRACT

The synthesis of silicalites and Mesoporous Silica Nanoparticles (MSN), which covalently incorporate original water-soluble photosensitizers for PDT applications is described. PDT was performed on MDA-MB-231 breast cancer cells. All the nanoparticles showed significant cell death after irradiation, which was not correlated with $^1O_2$ quantum yield of the nanoparticles. Other parameters are involved and in particular the surface and shape of the nanoparticles which influence the pathway of endocytosis. Functionalization with mannose was necessary to obtain the best results with PDT due to an active endocytosis of mannose-functionalized nanoparticles. The quantity of mannose on the surface should be carefully adjusted as a too high amount of mannose impairs the phototoxicity of the nanoparticles. Fluorescein was also encapsulated in MCM-41 type MSN in order to localize the nanoparticles in the organelles of the cells by confocal microscopy. The MSN were localized in lysosomes after active endocytosis by mannose receptors.

1. Introduction

Photodynamic therapy (PDT) has emerged as an alternative to chemo and radiotherapy for the treatment of early diagnosed and localized carcinoma (Pinthus et al., 2006). It involves the use of a photosensitizer (PS) which upon irradiation at a specific wavelength in the presence of oxygen molecules generates cytotoxic singlet oxygen and reactive oxygen species (ROS) which lead to irreversible destruction of cancer cells. Most of the PS are hydrophobic and have therefore a limited solubility in water. Nanoparticles have been developed to avoid this drawback and to improve PDT efficiency. Polymeric, metallic, semiconductor-based or silica-based nanoparticles have been described and this field has been reviewed recently (Bechet et al., 2008; Chatterjee et al., 2008; Couleaud et al., 2010). However, very few examples of nanoparticles encapsulating the PS through covalent linkage to avoid its premature release from the nanoparticle have been described (Cheng et al., 2009, 2010;

* Corresponding author. Tel.: +33 467143864.
** Corresponding author.
*** Corresponding author at: UMR 176 CNRS/Institut Curie, Institut Curie, Bât 110-112, Université Paris-Sud, F-91405 Orsay, France.
E-mail addresses: laurence.raehm@univ-montp2.fr (L. Raehm), morere@univ-montp2.fr (A. Morère), philippe.maillard@curie.u-psud.fr (P. Maillard).
[1] These authors contributed equally to this work.

0378-5173/$ – see front matter © 2010 Elsevier B.V. All rights reserved.
doi:10.1016/j.ijpharm.2010.10.004

Davydenko et al., 2006; Gu et al., 2005; Lai et al., 2008; McCarthy et al., 2006; Ohulchanskyy et al., 2007; Rossi et al., 2008; Tu et al., 2009). Those nanoparticles mostly possess a silica framework to attach the PS through alkoxysilane chemistry. In order to improve the uptake of the nanoparticles by tumor cells, so called third generation nanovectors have been also reported (Brevet et al., 2009; Cheng et al., 2010; Koo et al., 2006; Kopelman et al., 2005; Reddy et al., 2006; Ross et al., 2004; Zhang et al., 2007). Their aim is to target neoplasic cell membranes with a biomolecule anchored on the surface of the nanoparticles. Five examples of those vectors have been described for PDT applications (Brevet et al., 2009; Cheng et al., 2010; Koo et al., 2006; Kopelman et al., 2005; Reddy et al., 2006; Ross et al., 2004; Zhang et al., 2007) *in vitro* and *in vivo*. Among the variety of nanoparticles, Mesoporous Silica Nanoparticles (MSN) have very recently emerged as promising vectors for PDT applications (Brevet et al., 2009; Cheng et al., 2010; Cheng et al., 2009; Tu et al., 2009). Furthermore MSN were shown to reduce hemolytic activity towards mammalian red blood cells in comparison with non porous silica nanoparticles (Slowing et al., 2009). Thus nanoparticles gathering organized porosity, covalent incorporation of the PS and targeting of cancer cells with a biomolecule would be of high interest for PDT applications. We have synthesized third generation vectors with MSN which were proved to have a higher PDT efficiency than non-functionalized MSN (Brevet et al., 2009). We demonstrated that an active endocytosis pathway was involved in the uptake of the nanoparticles. Water solubility of the PS was brought by anionic sulfonate groups to improve its incorporation inside the MSN. We now present our work concerning the synthesis of nanoparticles with an organized porosity encapsulating cationic PS and we compare their cytotoxicity, phototoxicity with the nanoparticles encapsulating the anionic PS. MCM-41 type nanoparticles, MSN with a radial porosity (Derrien et al., 2008), and silicalite nanoparticles were prepared. The singlet oxygen quantum yield production of those nanoparticles was estimated and the phototoxicity was determined using breast cancer cell line MDA-MB-231. Functionalization of the surface of MCM-41 type MSN (encapsulating anionic PS) with mannose was performed and the quantity of mannose on the surface was correlated with the PDT activity of the nanoparticles. Finally, fluorescein dye was covalently incorporated in MCM-41 type MSN which were functionalized with mannose in order to characterize their endocytosis and subcellular localization in specific organelles.

2. Materials and methods

All solvents used were reagent grade. The following reagents have been abbreviated: 1,2-dichloroethane (1,2-DCE), dimethyl formamide (DMF), 1-hydroxybenzotriazole hydrate (HOBt), 1-(3-dimethylaminopropyl)-3-ethylcarbodiimide hydrochloride (EDC), triethylamine (Et_3N), diisopropylethylamine (DIPEA). Aminopropyltriethoxysilane (APTS), cetyltrimethylammonium bromide (CTAB) tetraethoxysilane (TEOS), fluorescein isothiocyanate (FITC), fetal bovin serum (FBS), 3-(4,5-dimethylthiazol-2-yl)-2,5-diphenyltetrazolium bromide (MTT), Dulbecco's modified Eagle's medium (DMEM). DMF was distilled under slow argon flow and kept over 4 Å sieves. Column chromatography was performed with the indicated solvents using E. Merck silica gel 60 (particle size 0.035–0.070 mm). Macherey-Nagel precoated plates (SIL G-200, 2 mm) were used for preparative thin-layer chromatography. Yields refer to chromatographically and spectroscopically pure compounds. ^{1}H NMR spectra were recorded on a Bruker AC-300 spectrometer at ambient temperature using an internal deuterium lock. Chemical shift values are given in ppm relative to tetramethyl silane (TMS). Acidic impurities in $CDCl_3$ were removed by treatment with anhydrous K_2CO_3. Quantitative UV–visible spectra were obtained using a UVIKON xm SECOMAM spectrometer (molar extinction coefficient values are given in L mmol^{-1} cm^{-1}). The electrospray mass spectra were performed with Water Micromass ZQ apparatus by infusion in water and the MALDI-TOF mass spectra with MALDI-TOF Voyager Spec equipped with a N_2 Laser emitting at 337 nm. Transmission Electron Microscopy (TEM) measurements were carried out with a JEOL 1200 EXII microscope at 100 kV. Dynamic Light Scattering (DLS) experiments were run using a Malvern spectrogoniometer, Autosizer 4800, with a 50 mW laser source operating at 532 nm. The samples were filtered in absolute EtOH through a 0.8 μm pore size filter. Specific surface areas were determined by Brunauer–Emmett–Teller (BET) method on a Micromeritics triStar analyser (using 75 points and starting from 0.01 as value for the relative pressure) and the average pore diameters were calculated by the BJH method.

2.1. Synthesis of porphyrin derivatives

2.1.1. 5-[p-(3-isoindoline-1′,3′-dione-propoxy)-phenyl]-10,15,20-tri-p-pyridyl-porphyrin **2**

Porphyrin **2** was synthesized from aldehyde **1** (6.2 g, 20 mmol) and 4-pyridinecarboxaldehyde (6.4 g, 60 mmol) which were poured into refluxing propionic acid (400 mL). Then freshly distilled pyrrole (5.36 g, 80 mmol) was added dropwise. The reflux was maintained for 2 h, and then the crude solution was evaporated to dryness under vacuum. A first chromatography on silica gel with a CH_2Cl_2/EtOH (100/5, v/v) eluent was performed to remove the tar. A second one performed with CH_2Cl_2 and increasing amounts of ethanol (0–10%) allowed separation of the six porphyrins. The titled porphyrin **2** was eluted as the third fraction with CH_2Cl_2/EtOH (94/6, v/v) and obtained after crystallization from CH_2Cl_2/methanol as blue powder (0.233 g, 5.7% yield). UV–vis spectrum in CH_2Cl_2: λ_{max}, nm (DO): 418.5 (1), 514.5 (0.61), 549 (0.31), 589 (0.25), 646 (0.16). ^{1}H NMR (300 MHz, $CDCl_3$) δ 9.05 (m, 6H, *meta*-pyridine), 8.95 (d, J = 4.7 Hz, 2H, pyrrole), 8.85 (s, 4H, pyrrole), 8.81 (d, J = 5 Hz, 2H, pyrrole), 8.16 (d, J = 5.8 Hz, 6H, *ortho*-pyridine), 8.07 (d, J = 8.4 Hz, 2H, *meta*-phenyl), 7.93 (dd, J = 3.1, 5.4 Hz, 2H, phthalimide), 7.76 (dd, J = 3.0, 5.4 Hz, 2H, phthalimide), 7.12 (d, J = 8 Hz, 2H, *ortho*-phenyl), 4.35 (t, 8 Hz, 2H, O–CH_2), 4.09 (t, 8 Hz, 2H, N–CH_2), 2.40 (m, 2H, CH_2), −2.87 (s, 2H, NH).

2.1.2. 5-[p-(3-aminopropoxy)-phenyl]-10,15,20-tri-p-pyridyl-porphyrin **3**

A mixture of porphyrin **2** (0.930 g, 1.13 mmol) and hydrazine monohydrate (0.71 mL, 23 mmol) was refluxed for 16 h, then stirred at room temperature for 24 h. Phthalhydrazide was precipitated by addition of aqueous HCl (10% solution) and filtered. The solution was neutralized by addition of aqueous NaOH (10% solution) and the porphyrin was extracted from the aqueous layer with a CH_2Cl_2/EtOH (95/5, v/v) mixture. After drying over sodium sulfate, filtration and evaporation of the solvents, the porphyrin **3** (0.760 g) was obtained pure as a blue powder in 97% yield and was used without other purification. UV–vis spectrum in CH_2Cl_2: λ_{max}, nm (ε L mmol^{-1} cm^{-1}): 418 (224.9), 515 (13.1), 550 (6.5), 590 (5.4), 647 (4.1). ^{1}H NMR (300 MHz, $CDCl_3$) δ 9.05 (m, 6H, *meta*-pyridine), 8.95 (d, J = 4.7 Hz, 2H, pyrrole), 8.85 (s, 4H, pyrrole), 8.81 (d, J = 5 Hz, 2H, pyrrole), 8.16 (d, J = 5.8 Hz, 6H, *ortho*-pyridine), 8.10 (d, J = 8.4 Hz, 2H, *meta*-phenyl), 7.31 (d, J = 8 Hz, 2H, *ortho*-phenyl), 4.38 (t, J = 8 Hz, 2H, O–CH_2), 3.09 (t, J = 8 Hz, 2H, N–CH_2), 2.14 (m, 2H, CH_2), −2.87 (s, 2H, NH).

2.1.3. 5-{p-[3-(2′,5′-dioxo-2′,5′-dihydro-1H-pyrrol-1′-yl)-N-3-phenoxypropyl)propanamide]-phenyl}-10,15,20-tri-p-pyridyl-porphyrin **5**

Compound **3** (160 mg, 0.23 mmol) was dissolved in methylene chloride (40 mL). HOBt (48 mg, 0.35 mmol), EDC (67 mg,

0.35 mmol), Et_3N (48 μL, 0.35 mmol) and 5-(2,5-dioxo-2,5-dihydro-pyrrol-1-yl)-propionic acid **4** (80 mg, 0.46 mmol) were added. The mixture was stirred under argon for 3 h at room temperature. The end of the reaction was controlled by silica gel thin layer chromatography eluted by a mixture of CH_2Cl_2/ethanol, (90/10, v/v). The crude solution was diluted by a mixture of CH_2Cl_2/ethanol (95/5, v/v) and washed by water (×3), dried over sodium sulfate, filtered and concentrated under vacuum. The crude product was purified by thin layer chromatography (Al_2O_3) eluted by a mixture of CH_2Cl_2/methanol (9/1, v/v). The titled compound **5** as obtained as blue powder after crystallization from a mixture CH_2Cl_2/ethanol/heptane (110 mg, 57% yield). UV–vis spectrum in CH_2Cl_2: λ_{max}, nm (ε L mmol^{-1} cm^{-1}): 418 (190.6), 516 (13.7), 550 (8.3), 591 (7.1), 652 (6.7). ^{1}H NMR (300 MHz, $CDCl_3$) δ 9.04 (d, J = 5.6 Hz, 6H, *meta*-pyridine), 8.92 (d, J = 5 Hz, 2H, pyrrole), 8.83 (s, 4H, pyrrole), 8.80 (d, J = 4.7 Hz, 2H, pyrrole), 8.13 (d, J = 5.7 Hz, 6H, *ortho*-pyridine), 8.10 (d, J = 8.5 Hz, 2H, *meta*-phenyl), 7.30 (d, J = 8.6 Hz, 2H, *ortho*-phenyl), 4.32 (t, J = 8 Hz, 2H, O–CH_2), 3.92 (t, J = 7.4 Hz, 2H, CH_2–N), 3.63 (t, J = 7.8 Hz, 2H, CH_2–NH–CO), 2.62 (t, J = 7 Hz, 2H, CH_2–CO–NH), 2.19 (t, 2H, CH_2), −2.87 (s, 2H, NH). ^{13}C NMR (300 MHz, $CDCl_3$) δ 170.65 (CON), 169.7 (CO–NH), 158.8 (*para*-phenyl), 150 (pyridine), 148.4 (*meta*-pyridine), 135.7 (*ortho*-phenyl), 134.3 (ethylene), 134 (phenyl), 131 (pyrrole), 129.4 (*ortho*-pyridine), 121.6 (*meso*-C), 117.4 (*meso*-C), 116.7 (*meso*-C), 112.8 (*meta*-phenyl), 66.6 (C–O–), 37.5 (C–NHCO), 34.9 (C–N), 34.3 (C–CONH), 29.2 (C–C–O). Electrospray mass spectrum: calc for $C_{51}H_{39}N_9O_4$ 841.9 found 842.66 M+1.

2.1.4. 5-{p-[3-(2′,5′-dioxo-2′,5′-dihydro-1H-pyrrol-1′-yl)-N-3-phenoxypropyl)propanamide]-phenyl}-10,15,20-tri-methyl-p-pyridynium-porphyrin tri chloride **6**

Porphyrin **5** (68 mg, 0.08 mmol) and methyl iodide (1 mL) were dissolved in DMF (20 mL) and stirred at room temperature for 3 h. The crude solution was concentrated under vacuum and diluted with methanol (10 mL). IRA 400 resin (0.9 g) was added and the suspension was slowly stirred for 1.5 h at room temperature. The solution was filtered and evaporated. The titled compound was obtained as blue crystals after crystallization from methanol/diethyl ether (80 mg, yield 100%). UV–vis spectrum in MeOH: λ_{max}, nm (ε L mmol^{-1} cm^{-1}): 427 (98.3), 518 (12), 557 (6.1), 593 (4.1), 652 (2.5). MALDI-TOF mass spectrum: calc for $C_{54}H_{48}N_9O_4Cl_3$ 993.38 found 886.44, M−3Cl$^-$, 887.44, M+H−3Cl$^-$.

2.2. Preparation of silicalite nanoparticles

2.2.1. Preparation of ***S9***

4.9 mg (4.45 μmol) of porphyrin **8** were stirred with APTS (2 μL, 1.5 equiv.) in EtOH (1 mL) overnight at RT. 14 mL of tetrapropylammonium hydroxide 1 M in water, 8.4 mL of $Si(OEt)_4$ and 2 mL of H_2O were then added under stirring. The solution was then heated for two days at 80 °C in a polyethylene flask, without stirring. The solution was then centrifuged (20 min 20,000 rpm) then the dispersion (ultrasounds)-centrifugation procedure was repeated two times (H_2O). The template was removed by exchange with HCl 12 N/EtOH (10/40, v/v) for 2 h at 60 °C, three times. Dispersion-centrifugation with H_2O (three times), then EtOH (two times) afforded the silicalites nanoparticles (225 mg). Specific surface area (100 m^2 g^{-1}), loading of **9** (0.424 μmol g^{-1}). DLS: 92 nm (EtOH).

2.2.2. Preparation of ***S11***

4 mg (4.35 μmol) of porphyrin **10** were reacted with isocyanatopropyltriethoxysilane (4.5 μL, 5 equiv.) and diisopropylethylamine (3.04 μL, 4 equiv.) in EtOH (1 mL) overnight. 14 mL of tetrapropylammonium hydroxide 1 M in water, 8.4 mL of $Si(OEt)_4$ and 2 mL of H_2O were then added under stirring. The solution was then heated for two days at 80 °C in a polyethylene flask, without stirring. The solution was then centrifuged (20 min, 20,000 rpm) then the dispersion-centrifugation procedure was repeated two times (H_2O). The template was removed by exchange with HCl 12 N/EtOH (10/40, v/v) for 2 h at 60 °C, three times. Dispersion-centrifugation with H_2O (three times), then EtOH (two times) afforded the silicalites nanoparticles (288 mg). Specific surface area (300 m^2 g^{-1}), loading of **9** (0.213 μmol g^{-1}), DLS 78 nm (EtOH).

2.3. Preparation of MCM-41 type nanoparticles

2.3.1. Preparation of ***MSN7***

8 mg (6.31 μmol) of porphyrine **6** were dissolved in 1 mL of methanol, 4.3 μL (21.78 μmol) of 3-mercaptopropyltrimethoxysilane were added. The reaction was stirred at room temperature for 12 h. 343 mg (0.95 mmol) of CTAB were dissolved in 20 mL of 0.2 M NaOH at 25 °C. The silylated porphyrin was added to this mixture. Then 1.75 mL (8 mmol) of TEOS were added dropwise. After 40 s, 128 mL of deionized water were added to the mixture. The reaction was stirred for 6 min at 25 °C then rapidly neutralized to pH 7 by addition of 0.2 M aqueous HCl. Nanoparticles were obtained after centrifugation (10 min, 20,000 rpm), put in suspension in ethanol under ultrasounds and then centrifuged. CTAB was extracted with 50 mL of solution of EtOH/HCl 12 N (4/1) for 2 h at 60 °C. After centrifugation, the extraction procedure was repeated two times, and then nanoparticles were put in suspension in water and centrifuged, until neutral pH. Specific surface area (1192 m^2 g^{-1}), loading of **7** (4.43 μmol g^{-1}).

2.3.2. Preparation of ***MSN9***

12 mg (0.011 mmol) of porphyrin **8** were dissolved in 1 mL of methanol, 4.8 μL of aminopropyltriethoxy silane (APTS) were added. The reaction was stirred at room temperature for 12 h. **MSN9** nanoparticles were then prepared as described for **MSN7.**

Specific surface area (1031 m^2 g^{-1}), loading of **9** (0.97 μmol g^{-1}).

2.3.3. Preparation of ***MSN11-3.5***

As previously described by Brevet et al. (2009).

2.3.4. Preparation of ***MSN11-5.8***

5 mg (5.44 μmol) of porphyrin **10** were dissolved in 1.5 mL of ethanol; 6.71 μL (5 equiv.) of isocyanatopropyltriethoxysilane and 3.8 μL (4 equiv.) of diisopropylethylamine were added. The reaction was stirred at room temperature for 12 h. 646 mg (1.8 mmol) of CTAB were dissolved in 40 mL of 0.2 M NaOH at 25 °C. The silylated porphyrine was added to this mixture. After 5 min, 3.5 mL (15.7 mmol) of TEOS were added dropwise. After 40 s, 260 mL of deionised water were added to the mixture. The reaction was stirred for 6 min at 25 °C then rapidly neutralized to pH 7 by addition of 0.2 M HCl. Nanoparticles were obtained after centrifugation (10 min. 20,000 rpm), put in suspension in ethanol under ultrasounds and then centrifuged. CTAB was extracted with 50 mL of solution of EtOH/HCl 12 N (4/1) for 2 h at 60 °C. After centrifugation, the extraction procedure was repeated two times, and then nanoparticles were put in suspension in water and centrifuged, until neutral pH. m = 907 mg. Specific surface area (1129 m^2 g^{-1}), loading of **11** (5.75 μmol g^{-1}).

2.4. Preparation of nanoparticles with radial porosity

2.4.1. Preparation of ***R11***

The monodisperse porphyrin-functionalised MSN with radial porosity were prepared using a *one-pot* method. 5 mg (5.44 μmol) of porphyrin **10** were dissolved in 1.5 mL of ethanol; 6.71 μL (5 equiv.) of isocyanatopropyltriethoxysilane and 3.8 μL (4 equiv.) of diisopropylethylamine were added. The reaction was stirred at room temperature for 12 h to lead to **11**. In a typical synthesis

procedure 1.36 mmol dodecyltrimethylammonium bromide was dissolved in 100 g solution of water and ethylene glycol. Then functionalized porphyrin **11** was added and the mixture was stirred at 398 K. After complete micellar solubilisation of the porphyrin precursor, the addition of 3 mmol of tetramethoxysilane was performed under vigorous stirring. The mixture was stirred overnight and the resulting precipitate was recovered by centrifugation, dried and washed in acidic condition (50 mL of solution of EtOH/HCl 12 N (4/1) for 2 h at 60 °C) to extract the surfactant. Specific surface area (1115 $m^2 g^{-1}$), loading of **11** (6.70 μmol g^{-1}).

2.5. Preparation of MCM-41 type MSN functionalized with NH_2

2.5.1. Preparation of ***MSN11-3.5-NH$_2$***

As previously described by Brevet et al. (2009).

2.5.2. Preparation of ***MSN11-5.8-NH$_2$***

700 mg of **MSN11-5.8** were put in suspension in 17 mL H_2O. 952 μL of APTS was diluted in 5 mL of EtOH. This solution was added to the nanoparticles suspension. The pH was adjusted to 7 by addition of 0.2 M HCl (15 mL). The reaction was stirred at RT for 20 h. Nanoparticles were centrifuged (10 min. 20000 rpm) and washed with EtOH and dried under vacuum. m = 813 mg. Microanalysis: % C 8,69; % H 2,95; % N 2,41. Loading of 1.8 mmol of APTS per gram of **MSN11-5.8-NH$_2$**. Specific surface area (479 $m^2 g^{-1}$, pore size 2.4 nm).

2.6. Preparation of MCM-41 type MSN functionalized with mannose

2.6.1. Preparation of ***MSN11-3.5-0.1***

As previously described by Brevet et al. (2009).

2.6.2. Preparation of ***MSN11-5.8-0.1***

16.4 mg of **MSN11-5.8-NH$_2$** were put in suspension in 2 mL EtOH. 1.17 mg of p-[N-(2-Ethoxy-3,4-dioxycyclobut-1-enyl)amino]phenyl-α-D-mannopyranoside (0.1 equiv./NH_2) were dissolved in 500 μL EtOH/H_2O 3/2. This solution was added dropwise to the suspension of **MSN11-5.8-NH$_2$**, and then 100 μL of Et_3N were added. The reaction was stirred for 15 h. The reaction was then centrifuged (20 min, 20,000 rpm), redispersed in H_2O and centrifuged three times, redispersed in EtOH and centrifuged three times. m = 11.7 mg of nanoparticles were obtained. Titration of mannose: 0.16 mmol g^{-1}.

2.6.3. Preparation of ***MSN11-5.8-0.25***

150 mg of **MSN11-5.8-NH$_2$** were put in suspension in 10 mL EtOH. 27 mg of p-[N-(2-Ethoxy-3,4-dioxycyclobut-1-enyl)amino]phenyl-α-D-mannopyranoside (0.25 equiv./NH_2) were dissolved in 10 mL EtOH/H_2O 3/2. This solution was added dropwise to the suspension of **MSN11-5.8-NH$_2$**, and then 500 μL of Et_3N were added. The reaction was stirred for 18 h. The reaction was then centrifuged (20 min, 20,000 rpm), redispersed in H_2O and centrifuged three times, redispersed in EtOH and centrifuged three times. m = 134 mg of nanoparticles were obtained. Specific surface area (526 $m^2 g^{-1}$, pore size 2 nm). Titration of mannose: 0.38 mmol g^{-1}.

2.6.4. Preparation of ***MSN11-5.8-0.5***

The same procedure as for **MSN11-5.8-0.25** with 54 mg (0.5 equiv./NH_2) of p-[N-(2-Ethoxy-3,4-dioxycyclobut-1-enyl) amino]phenyl-α-D-mannopyranoside gave m = 145 mg of nanoparticles. Specific surface area (431 $m^2 g^{-1}$, pore size 2 nm). Titration of mannose: 0.54 mmol g^{-1}.

2.6.5. Preparation of ***MSN11-5.8-1***

The same procedure as for **MSN11-5.8-0.25** with 107 mg (1 equiv./NH_2) of p-[N-(2-Ethoxy-3,4-dioxycyclobut-1-enyl) amino]phenyl-α-D-mannopyranoside gave m = 155 mg of nanoparticles. Specific surface area (285 $m^2 g^{-1}$, pore size 1.9 nm). Titration of mannose: 0.61 mmol g^{-1}.

2.6.6. Preparation of ***MSN11-5.8-2***

The same procedure as for **MSN11-5.8-0.25** with 210 mg (2 equiv./NH_2) of p-[N-(2-Ethoxy-3,4-dioxycyclobut-1-enyl) amino]phenyl-α-D-mannopyranoside gave m = 141 mg of nanoparticles. Specific surface area (201 $m^2 g^{-1}$, pore size 1.7 nm). Titration of mannose: 0.74 mmol g^{-1}.

2.7. Preparation of FITC-functionalized MCM-41 type MSN

2.7.1. Preparation of ***MSN-FITC***

10 mg (2.57×10^{-2} mmol) of fluoresceine isothiocyanate (FITC) were dissolved in 1.5 mL of absolute ethanol. 5.33 μL (2.57×10^{-2} mmol) of APTS were added. The reaction was stirred at room temperature for 12 h. 686 mg (15.6 mmol) of CTAB were dissolved in 40 mL of 0.2 M NaOH at 25 °C. The preceding solution was added to this mixture. Then 3.5 mL (1.57 mmol) of TEOS were added dropwise. After 40 s, the mixture was diluted with 260 mL of deionised water at 25 °C. The reaction was stirred for 6 min at 25 °C then rapidly neutralized to pH 7 by addition of 0.2 M HCl. Nanoparticles were obtained after centrifugation (10 min, 20,000 rpm). Nanoparticles were dispersed in EtOH then centrifuged. Surfactant was removed by extraction with NH_4NO_3 solution (0.75 mg NH_4NO_3 dissolved in 150 mL of 95% ethanol) for 15 min at 60 °C. After centrifugation, the extraction procedure was repeated two times. UV–vis titration gave a loading of 1.97 μmol of FITC per gram of **MSN-FITC**.

2.8. Preparation of FITC-functionalized MCM-41 type MSN with NH_2

2.8.1. Preparation of ***MSN-FITC-NH$_2$***

400 mg of **MSN-FITC** were put in suspension in 10 mL H_2O. 626 μL of APTS was diluted in 5 mL of EtOH. This solution was added to the nanoparticles suspension. The pH was adjusted to 7 by addition of 0.2 M HCl. The reaction was stirred at RT for 20 h. Nanoparticles were centrifuged (10 min, 20000 rpm) and washed with EtOH and dried under vacuum.

Microanalysis: %C 5.78, %H 3.29, %N 1.58. Loading of 1.13 mmol of APTS per gram of **MSN-FITC-NH$_2$**.

2.9. Preparation of FITC-functionalized MCM-41 type MSN with mannose

2.9.1. Preparation of ***MSN-FITC-0.1***

100 mg of **MSN-FITC-NH$_2$** were put in suspension in 5 mL EtOH. 7.11 mg (1.8×10^{-2} mmol) of p-[N-(2-Ethoxy-3,4-dioxycyclobut-1-enyl)amino]phenyl-α-D-mannopyranoside were dissolved in 5 mL EtOH/H_2O (50/50). This solution was added dropwise to the suspension of NP. 500 μL of triethylamine (Et_3N) were added and the suspension was stirred for 18 h. After centrifugation (10 min, 20,000 rpm), nanoparticles were washed with water (3 cycles), then with EtOH twice. They were dried under vacuum. Titration (resorcinol/H_2SO_4) gave 0.035 mmol of mannose per gram of **MSN-FITC-0.1.**

2.9.2. Preparation of ***MSN-FITC-0.5***

MSN-FITC-0.5 were prepared as described for **MSN-FITC-NH$_2$** 0.1, 35.5 mg (0.9×10^{-4} mol) of p-[N-(2-Ethoxy-3,4-dioxycyclobut-1-enyl)amino]phenyl-α-D-mannopyranoside were utilized. Titra-

tion (resorcinol/H_2SO_4) gave 0.087 mmol of mannose per gram of **MSN-FITC-0.5.**

2.10. Determination of singlet oxygen quantum yield [$\Phi(^1O_2)$] (DeRosa and Crutchley, 2002)

Excitation occurred with a Xe-arc, the light was separated in a SPEX 1680, 0.22 μm double monochromator. The detection at 1270 nm was done through a PTI S/N 1565 monochromator, and the emission was monitored by a liquid nitrogen-cooled Ge-detector model (EO-817L, North Coast Scientific Co). The absorbance of the reference solution (Rose Bengal in EtOH $\Phi(^1O_2) = 0.681$ and the sample solution (at 418 nm) were set equal (between 0.2 and 0.5) by dilution.

2.11. Cell culture conditions and phototoxicity assay

Human breast cancer cells (MDA-MB-231) were maintained in Dulbecco's modified Eagle's medium (DMEM) supplemented with 10% of fetal bovine serum (FBS), phenol red, glutamine and 50 μg mL^{-1} gentamycin, in humidified atmosphere at 37 °C and 5% CO_2.

Cancer cells were seeded into 96-well plates at 2×10^4 cells/well in 100 μL of culture medium and allowed to grow for 24 h. Then cells were incubated 24 h with or without 20 μg mL^{-1} of nanoparticles. After incubation with nanoparticles, cells were washed twice, maintain in fresh culture medium and then submitted or not to laser irradiation (630–680 nm; 6 mW cm^{-2}) for 40 min. Two days after irradiation, MTT assay was performed to evaluate the cytotoxicity of nanoparticles. Briefly, cells were incubated in the presence of 0.5 mg mL^{-1} MTT during 4 h to determine mitochondrial enzyme activity. Then MTT precipitates were dissolved in 150 μL ethanol/DMSO (1:1) solution and absorbance was read at 540 nm.

2.12. Confocal analysis of fluorescent nanoparticles

Stock solutions of nanoparticles were dissolved in EtOH at the concentration of 1 mg mL^{-1} and were further added in serum free culture medium at 20 μg mL^{-1}. All compounds were protected from light throughout the experiment and their fluorescence activities were regularly verified.

The day prior to the experiment, MDA-MB-231 cells were seeded onto bottom glass dishes (World Precision Instrument, Stevenage, UK) at a density of 10^6 cells/cm^2. On the day of the experiment, cells were washed once and incubated in 1 mL red-free medium containing fluorescent labeled nanoparticles at a concentration of 20 μg mL^{-1} for 24 h. 30 min before the end of incubation, cells were loaded with Hoechst 33342 (Invitrogen, Cergy Pontoise, France) for nuclear staining at a final concentration of 5 μg mL^{-1}.

For the lysosome labeling, 3 h before the end of the experiment, 50 nM of lysotracker red DND-99 (Invitrogen) was added to phenol red-free DMEM. Before visualization, cells were washed gently with phenol red-free DMEM. Cells were then scanned with a LSM 5 LIVE confocal laser scanning microscope (Carl Zeiss, Le Pecq, France), with a slice depth (Z stack) of 0.67 μm.

The distributions of fluorescent nanoparticles were analyzed by CLSM using nucleus and lysosome markers. Merged images of fluorescent nanoparticles and lysosome marker allow the determination of the nanoparticle level into lysosomes. The image threshold was obtained for both channels and the extent of true co-localization (yellow pixels in merged image) was analyzed using the Manders overlap co-localization coefficient with green channel (co-localization module, Zeiss MicroImaging). A value of 1 is high co-localization and a value of 0 is low co-localization. Co-localization coefficient represents the sum of co-localizing pixels (in merged image) as compared to the overall sum of pixels above the threshold in the red channel (lysosomal marker). Thus, this coefficient generates normalized scores in which the effect of lysosome quantity is substantially reduced. A value of 1 indicates a high quantity of nanoparticles into lysosomes, whereas a value of 0 indicates the absence of nanoparticles into lysosomes.

2.13. Statistical analysis

Statistical analysis was performed using the Student's *t*-test to compare paired groups of data. A *P*-value of <0.05 was considered to be statistically significant.

3. Results and discussion

3.1. Syntheses of porphyrin derivatives

The syntheses of two cationic photosensitizers **7**, **9** possessing three methyl-pyridinium groups were performed. Porphyrin **7** was prepared as follows: compound **1** (1 equiv.) obtained by the method described by Dick et al. (1992) from *para*-hydroxybenzaldehyde and 2-(4-bromobutyl)isoindoline-1,3-dione under Williamson's conditions, was condensed, by standard Adler's procedure, with *para*-pyridinaldehyde (3 equiv.) and pyrrole (4 equiv.) to give after purification by chromatography porphyrin **2** in 5.7% yield. (Perrée-Fauvet et al., 1996) Derivative **3** (Scheme 1) was obtained from compound **2** by treatment with hydrazine in water and reflux in quantitative yield.

The reaction of porphyrin **3** and acid **4** in the presence of 1-hydroxybenzotriazole hydrate (HOBt), 1-(3-dimethylaminopropyl)-3-ethylcarbodiimide hydrochloride (EDC) and triethylamine as coupling agents in methylene chloride gives compound **5** in 57% yield. This last compound was treated by methyl iodide to give quantitatively, after treatment with IRA 400 resin, chloride salt of water-soluble porphyrin **6** (Scheme 2). Porphyrin **6** was silylated into porphyrin **7** by reaction with mercaptopropyltrimethoxysilane in methanol.

Porphyrin **8** was synthesized as described previously (Sutton et al., 2002). Porphyrin **8** was silylated by reaction with aminopropyltriethoxysilane in EtOH (Scheme 3).

Silylated anionic porphyrin **11** was prepared from porphyrin **10** as described (Brevet et al., 2009) (Scheme 4) and was used to compare its behavior with silylated cationic porphyrins **7** and **9**.

All porphyrins were characterized by ^1H NMR and UV–visible spectroscopy, compound **5** by electro spray mass spectroscopy and compound **6** by MALDI-TOF mass spectroscopy.

3.2. Syntheses of silica-based nanoparticles with organized porosity

Different kinds of nanoparticles were synthesized: silicalites **S9**, **S11**, MCM-41 type nanoparticles **MSN7**, **MSN9**, **MSN11** and MSN with radial porosity **R11**. Silicalite nanoparticles were obtained by in situ encapsulation of silylated porphyrin **9** for **S9** or **11** for **S11** following a recently described synthesis (Lerouge et al., 2009) and the template was removed by treatment with a solution of HCl 12 N in EtOH at 60 °C. Those nanoparticles were highly crystalline as shown by X-ray diffraction (data not shown). Dynamic light scattering (DLS) showed diameters of 92 nm and 78 nm for **S9** and **S11** respectively. The N_2 adsorption–desorption BET confirmed the organized microporosity with specific surface areas of 100 $m^2\ g^{-1}$ and 300 $m^2\ g^{-1}$ respectively. Titration by UV–visible spectroscopy showed loading of 0.424 μmol of **9** per gram of **S9** and 0.213 μmol of **11** per gram of **S11**. The quantum yield of singlet oxygen production obtained by $^1O_2$ phosphorescence measurements in EtOH, with Rose Bengal used as the standard reference, was calculated to

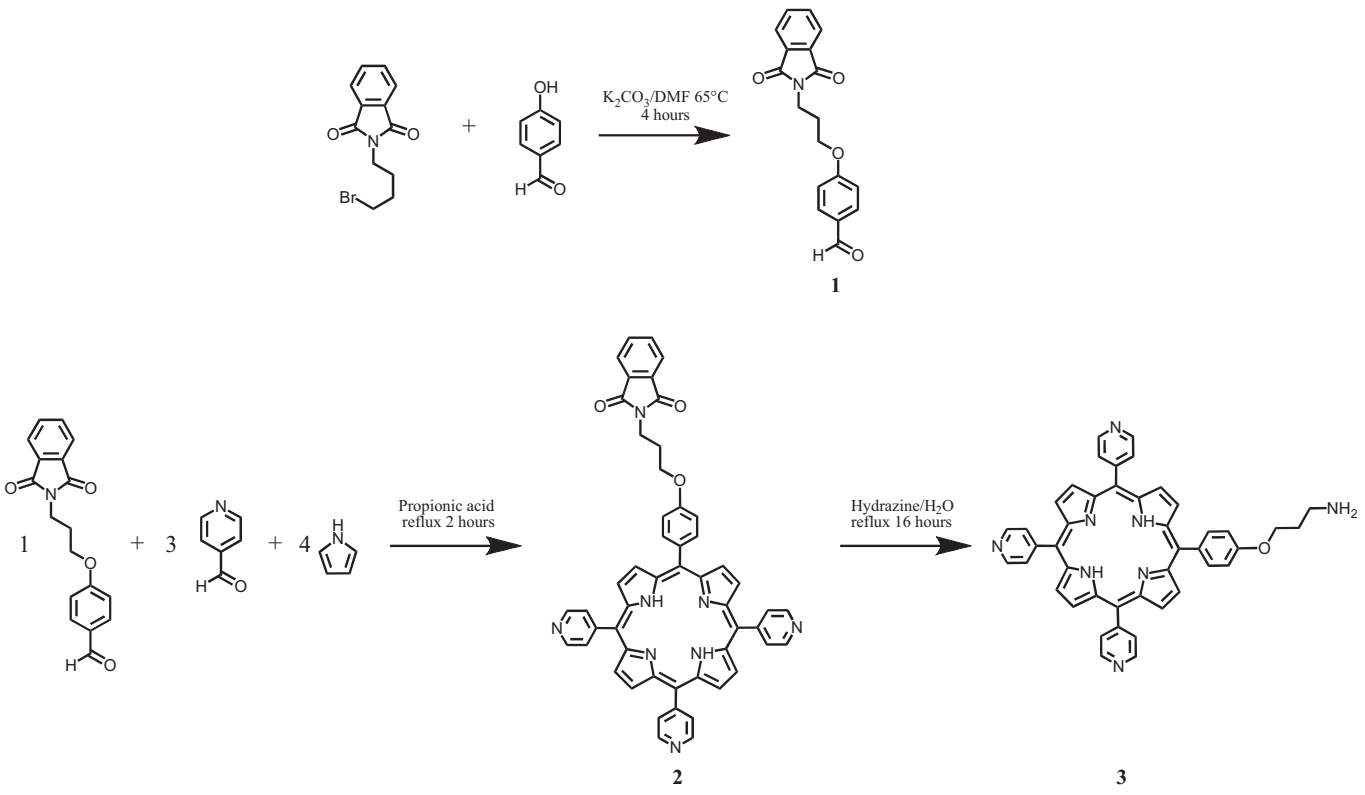

Scheme 1. Synthesis of derivative **3**

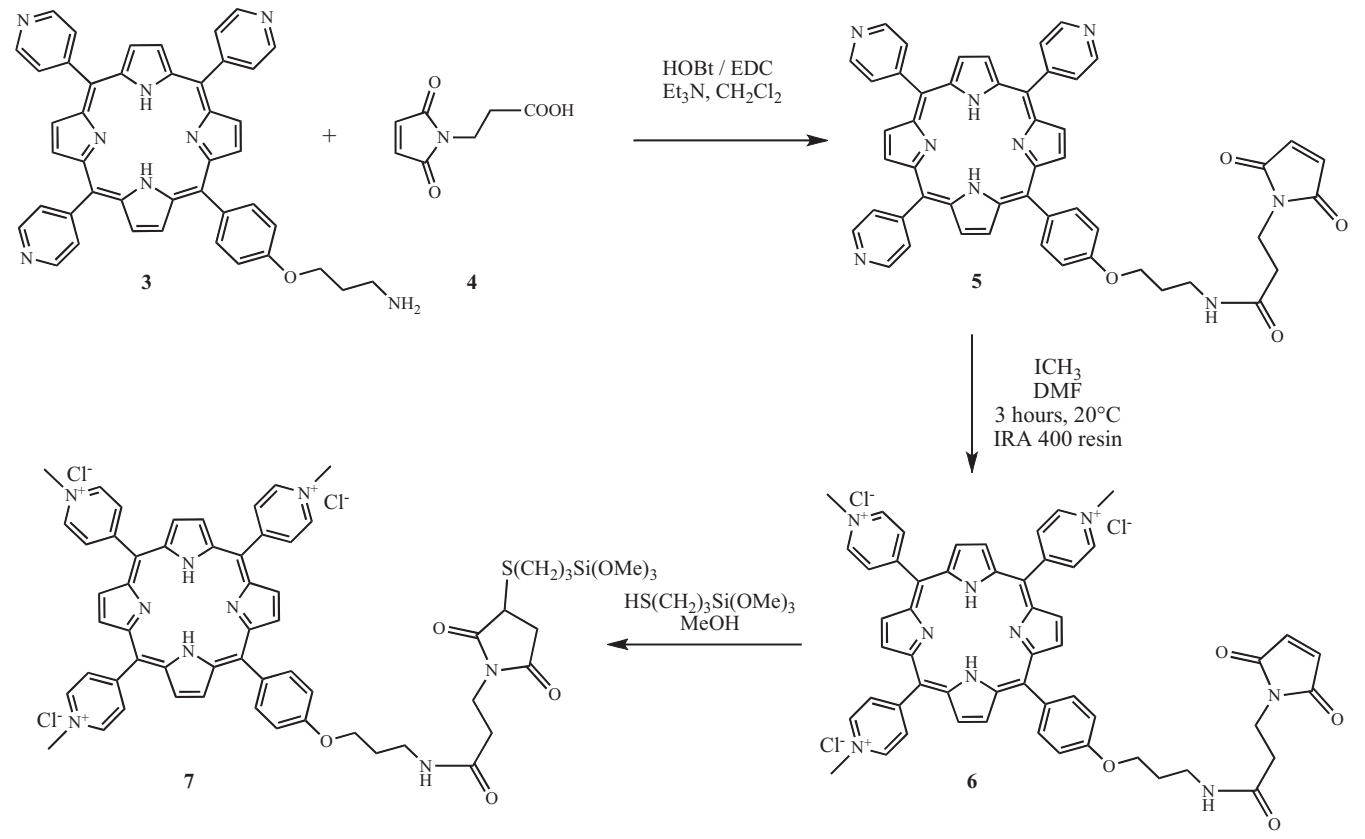

Scheme 2. Synthesis of silylated porphyrin **7**

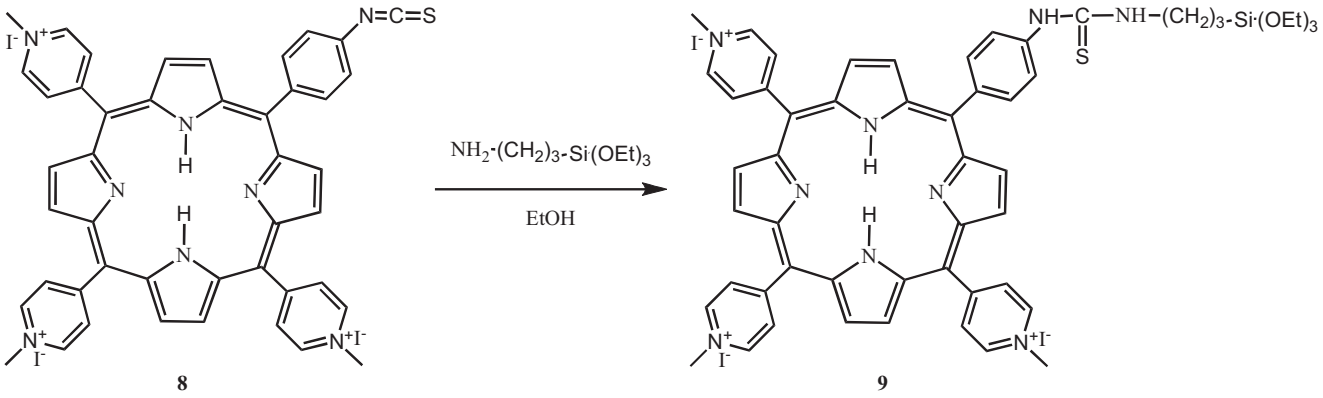

Scheme 3. Silylation of porphyrine **8**

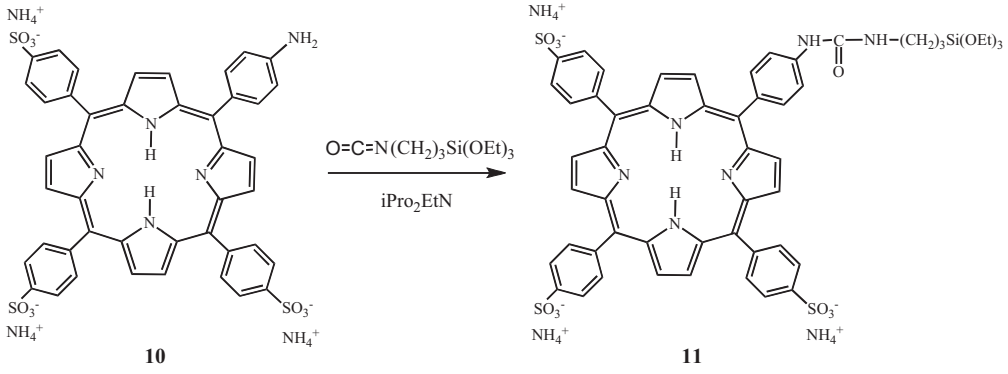

Scheme 4. Silylated porphyrine **11**

be 31% for **S11** and was too low to be calculated for **S9**. **MSN7**, **MSN9**, **MSN11** were synthesized by *in situ* encapsulation of porphyrins **7**, **9**, **11** respectively following recently described methods (Brevet et al., 2009; Lebret et al., 2008). The surfactant was removed as above. BET confirmed the organized mesoporosity of **MSN7** and **MSN9** with specific surface areas of 1192 $m^2 g^{-1}$ and 1031 $m^2 g^{-1}$, pore diameters of 2 nm and 2.3 nm respectively. TEM showed an average diameter of 130 nm for **MSN7** and **MSN9**. Titration by UV–visible spectroscopy showed loading of 4.43 μmol of **7** per gram of **MSN7** and 0.97 μmol of **9** per gram of **MSN9**. The quantum yield of singlet oxygen production was calculated to be 58% for **MSN7** and 60% for **MSN9**. Concerning **MSN 11** two batches of nanoparticles were prepared. The first batch (**MSN11-3.5**) was described in our previous work (Brevet et al., 2009) with 3.50 μmol of **11** per gram of nanoparticles. For the second batch (**MSN11-5.8**) we slightly modified the conditions of synthesis (hydrolysis of the triethoxysilane moiety) to get a higher content of porphyrin inside the MSN. Titration by UV–visible spectroscopy showed loading of 5.80 μmol of **11** per gram of nanoparticles, BET showed a specific surface area of 1129 $m^2 g^{-1}$ and pore diameters of 2.5 nm. As the specific surface area was higher than with **MSN11-3.5**, the porphyrin moiety was mainly located in the walls of the silica framework due to its water solubility. TEM showed average diameters of 100 nm. Another type of mesoporous silica nanoparticle **R11** with radial porosity was prepared as well. The synthesis conditions were different from that of MCM-41 type nanoparticles (TMOS was used as the silica source and dodecyltrimethylammonium bromide was used as the surfactant). The surfactant was eliminated as above. BET confirmed the organized mesoporosity with a specific surface area of 1115 $m^2 g^{-1}$ and a pore diameter of 2.4 nm. SEM showed an average diameter of 150 nm for **R11**. Titration by UV–visible spectroscopy showed loading of 6.70 μmol of **11** per gram of **R11**. The quantum yield of singlet oxygen production was calculated to be 65% for **R11**, the highest obtained with the nanoparticles. Table 1 summarizes the characteristics of the nanoparticles.

3.3. Phototoxicity

Human breast cancer cells (MDA-MB-231) were incubated with the photo-activable nanoparticles at 20 μg mL^{-1} for 24 h at 37 °C and irradiated for 40 min (630–680 nm; 6 mW cm^{-2}) or not.

The 3-(4,5-dimethylthiazol-2-yl)-2,5-diphenyltetrazolium bromide (MTT) assay (Mosmann, 1983), as described in experimental part, was then performed after two days to assess the cytotoxicity of the nanoparticles (Table 2).

The nanoparticles were not cytotoxic at 20 μg mL^{-1} in the dark. After irradiation, all the nanoparticles showed photocytotoxicity which is in agreement with $^1O_2$ formation. Nevertheless, **R11**

Table 1
Characteristics of nanoparticles.

Nanoparticles	S9	S11	MSN7	MSN9	MSN11-3.5	MSN11-5.8	R11
BET ($m^2 g^{-1}$)	100	300	1192	1031	860	1129	1115
Pore diameter (nm)	–	–	2.0	2.3	2.2	2.5	2.4
Porphyrin (μmol g^{-1})	0.42	0.21	4.43	0.97	3.50	5.80	6.70
TEM/SEM (nm)	90	80	130	130	100	100	150

Table 2
Cell viabilities (% control) of MDA-MB-231 breast cancer cells.

Nanoparticles	S9	S11	MSN7	MSN9	MSN11-3.5	MSN11-5.8	R11
No irradiation% of living cells	98 ± 4	96 ± 5	99 ± 4	103 ± 6	97 ± 4	103 ± 9	98 ± 3
Irradiation% of living cells	48 ± 5*	55 ± 6*	52 ± 7*	43 ± 5*	64 ± 4*	40 ± 8*	73 ± 4*
Quantum yield of $^1O_2$ production (EtOH ± 5%)	Not calculable	31	58	60	58	46	65

Cells were incubated for 24 h with nanoparticles, submitted or not to irradiation, and $^1O_2$ quantum yield (%) was assayed as described in experimental part.
* $p < 0.05$ statistically different from control.

showed the lowest photocytotoxicity whereas its $^1O_2$ quantum yield was the highest of the tested nanoparticles. **S9** is highly phototoxic, but, even if we could observe the characteristic phosphorescence of $^1O_2$ at 1270 nm in ethanol, it was not possible to estimate properly the quantum yield due to both the low porphyrin charge and the high diffusion.

The $^1O_2$ quantum yield of **MSN11-3.5** was higher than that of **MSN11-5.8**, (which may be due to porphyrin aggregation with **MSN11-5.8**) but the photoactivity of **MSN11-5.8** was higher. The efficiency of PDT is thus not only correlated with $^1O_2$ quantum yield production, as already observed by Vicente and colleagues (Hao et al., 2008) with a carboranyl-chlorin derivative where the quantum yield of $^1O_2$ production was very low (10%) and the PDT activity of the chlorin was high. The authors suggested that other mechanisms of cell death than $^1O_2$ production occurred (electron transfer from the triplet state). In our case, the pathway of endocytosis of the nanoparticles could have an important impact on the PDT efficacy as well. The surface and shape of the nanoparticles are different for crystalline silicalite, MCM-41 type nanoparticles or mesoporous nanoparticles with radial porosity and this has been demonstrated to have an important biological effect (Hu et al., 2009; Huang et al., 2010; Slowing et al., 2009), particularly on cellular uptake and cell function (Huang et al., 2010).

3.4. Functionalization of MCM-41 type nanoparticles with NH_2 and mannose, phototoxicity

In order to improve the selectivity of the nanoparticles for cancer cells, **MSN11-3.5** and **MSN11-5.8** nanoparticles were functionalized with aminopropyltriethoxysilane (1.5 mmol g^{-1}, (Brevet et al., 2009) and 1.72 mmol g^{-1} respectively) leading to nanoparticles **MSN11-3.5-NH$_2$** and **MSN11-5.8-NH$_2$**. Squarate mannose was then grafted to target mannose receptors at the surface of cancer cells (Scheme 5). Mannose (0.1 equiv. of mannose per NH_2 group) was reacted with **MSN11-3.5-NH$_2$** to lead to **MSN-11-3.5-0.1** (Brevet et al., 2009) with a quantity of mannose of 0.18 mmol g^{-1}. Concerning **MSN11-5.8-NH$_2$**, a grafting study of squarate mannose was performed between 0.1 and 2 equiv. of mannose per NH_2 to determine the optimum amount of mannose on the surface of **MSN11-5.8-X** (**X**: equivalent number of squarate mannose varying from 0.1 to 2) to get the highest efficiency during PDT experiments (Table 3).

PDT experiments were first performed with **MSN11-3.5**, **MSN11-3.5-NH$_2$**, **MSN11-3.5-0.1** at different times of incubation

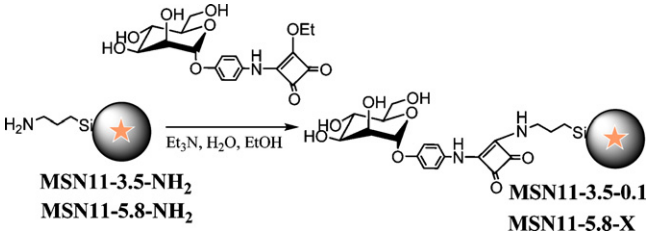

Scheme 5. Functionalization of **MSN11**

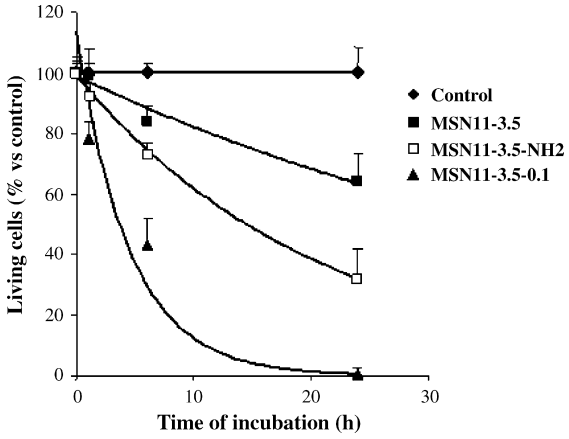

Fig. 1. Effect of incubation time on the cytotoxicity of nanoparticles on MDA-MB-231 cancer cells. Cells were incubated or not (♦) with 20 μg mL^{-1} of **MSN11-3.5** (■) or **MSN11-3.5-NH$_2$** (□) or **MSN11-3.5-0.1** (▲) at different times and then, submitted to laser irradiation (40 min; 6 mW cm^{-2}). MTT assay was realized two days after irradiation. The remaining living cells were expressed as a percent of non-irradiated control cells. Data are mean ± SD of three independent experiments.

(1 h, 6 h, 24 h). Results showed that 24 h of incubation were necessary to get high PDT efficiency. Unfunctionalized **MSN11-3.5** were less efficient than **MSN11-3.5-NH$_2$**. The best results were obtained with **MSN11-3.5-0.1** which induced 99% of cell death (Brevet et al., 2009) with a 24 h of incubation (Fig. 1). This effect is clearly due to differences in the endocytosis pathway of the nanoparticles. Indeed the uptake of MSN without functionalization on the surface has been demonstrated to be mediated by a clathrin-pitted mechanism (Huang et al., 2005). Clathrin is a protein that coats the vesicles which are going to be part of the cell membrane. These vesicles form domains of the plasma mem-

Table 3
Functionalization and cytotoxic effect of MSN11 anchored with increasing mannose concentrations on MDA-MB-231 cancer cells.

Nanoparticles	MSN10-0.1	MSN10-0.25	MSN10-0.5	MSN10-1	MSN10-2
Titration of mannose (mmol g^{-1})	0.16	0.38	0.545	0.61	0.74
No irradiation % living cells)	98 ± 6	104 ± 4	98 ± 4	106 ± 5	102 ± 4
Irradiation (% living cells)	27 ± 7**	56 ± 8*	64 ± 8*	64 ± 10*	73 ± 10*

Cells were incubated with 20 μg mL^{-1} of nanoparticles covered with different concentrations of mannose for 24 h and then, submitted to laser irradiation (40 min; 6 mW cm^{-2}). MTT assay was performed two days after irradiation. Values represent the percent of living cells as compared to untreated control considered as 100%. Data are mean ± SD of three independent experiments.
* $p < 0.05$ statistically different from control.
** $p < 0.05$ statistically different from other MSN.

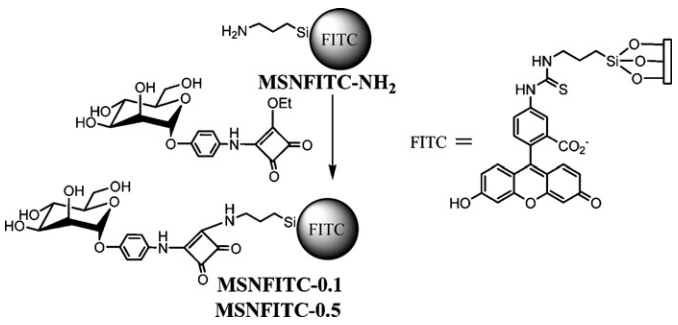

Scheme 6. Functionalization of **MSN-FITC** with mannose.

brane (pits). A caveolae dependent mechanism of endocytosis with amino-functionalized MSN has been demonstrated (Slowing et al., 2006). Caveolae are protein and lipid rich structures of 50–100 nm which allow invagination of the plasma membrane and endocytosis of the amino-functionalized MSN. This mechanism is clathrin independent. The uptake of **MSN11-3.5-0.1** is mediated by mannose receptors (Brevet et al., 2009) over-expressed at the cell membrane and this later way of endocytosis seems to be the most efficient. After 24 h of incubation of **MSN11-3.5-0.1** by this pathway of endocytosis then irradiation, all the cancer cells were killed.

3.5. Phototoxicity of MCM-41 type nanoparticles with different loading of mannose

From 0.1 to 2 equiv. of squarate mannose were then reacted with **MSN11-5.8-NH_2** (Table 2) and the amount of anchored residues was titrated by resorcinol/H_2SO_4 (Park et al., 2008).

The photodynamic activity of **MSN11-5.8-0.1** to **MSN11-5.8-2** was estimated on MDA-MB-231 cancer cells. Table 3 shows that high mannose concentrations anchored at MSN surface impair the toxicity of the nanoparticles. The presentation and density of the ligand in the recognition by lectins is known to strongly influence the binding process (De la Fuente and Penades, 2006). In our case, the loss of efficiency could be due to an excessive steric hindrance, reducing a possible clustering effect (Ballut et al., 2009) between mannose on the nanoparticles and lectins. Thus a low amount of mannose of 0.16–0.18 mmol g^{-1} is critical to get high efficiency for PDT experiments.

3.6. FITC-functionalized MCM-41 type nanoparticles, confocal microscopy studies

In order to analyze the cell distribution of MSN functionalized or not with squarate mannose, we incorporated fluorescein isothiocyanate (Lin et al., 2005) (FITC) instead of porphyrin derivatives inside the MSN (Scheme 6). Indeed FITC is suitable for the use of confocal microscopy to localize the nanoparticles inside the organites of the cells. **MSN-FITC** were prepared using a procedure similar to the preparation of **MSN7**. They were then grafted with aminopropyltriethoxysilane to lead to **MSN-FITC-NH_2**.

α-Mannose was then grafted on the surface of **MSN-FITC-NH_2**. Two kinds of nanoparticles were synthesized with 0.1 and 0.5 equiv.

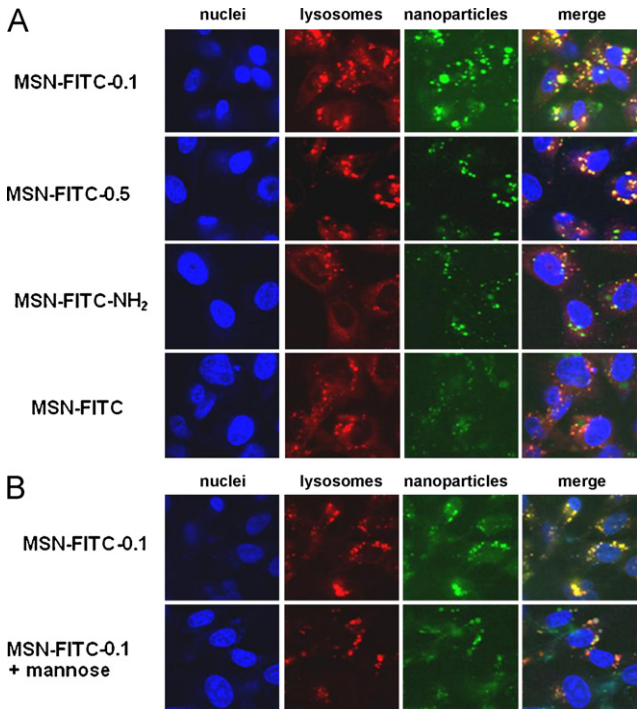

Fig. 2. Confocal microscopy images of living MDA-MB-231 breast cancer cells incubated with nanoparticles. To visualize intracellular nanoparticles, cells were stained with nucleus and lysosome markers. (A) Co-localization of nanoparticles functionalized or not with mannose with the lysosome marker after 24 h of incubation at 37 °C. (B) Co-localization of nanoparticles functionalized with mannose in the absence or presence of 10 mM mannose. Data are from one representative of three independent experiments.

of mannose per NH_2 respectively. Titration gave 0.035 mmol of mannose per gram of **MSN-FITC-0.1** and 0.087 mmol of mannose per gram of **MSN-FITC-0.5**.

The cell distribution of MSN internalized by cancer cells was studied using FITC labelled nanoparticles (**MSN-FITC**; **MSN-FITC-NH_2**; **MSN-FITC-0.1**; **MSN-FITC-0.5**). MSN functionalized or not with mannose were incubated for 24 h with MDA-MB-231 cells and then nucleus and lysosomes were stained with Hoechst 33342 and lysotracker respectively as described in Section 2 (Fig. 2). Merged image of lysosomes and **MSN-FITC** showed that **MSN-FITC-0.1** were more efficiently internalized and located in lysosomes, than **MSN-FITC-NH_2** and than unfunctionalized **MSN-FITC**. In addition **MSN-FITC-0.5** are less addressed to lysosomes than **MSN-FITC-0.1** confirming that a too high concentration of mannose anchored at MSN surface impairs the internalization (Fig. 2A). The internalization of **MSN-FITC-0.1** was also analyzed in presence or in absence of a mannose excess. Fig. 2B shows that a pre-incubation in culture medium with a mannose excess induces a strong decrease in the internalization of **MSN-FITC-0.1** demonstrating that their localization into the lysosomes of cancer cells is due to an active endocytosis involving mannose receptor recognition. Co-localization values as reported in Table 4, indicated the higher lysosomal location of **MSN-FITC-0.1**.

Table 4
Quantification of nanoparticles localized into lysosomes.

Nanoparticles	MSN-FITC	MSN-FITC-NH2	MSN-FITC-0.5	MSN-FITC-0.1
Manders coefficient	0.94	0.85	0.91	0.98
Co-localization coefficient	0.29	0.46	0.69	0.82

Cells were incubated with 20 μg mL^{-1} of **MSN-FITC** functionalized or not with mannose for 24 h. Manders coefficient indicates the degree of co-localization (yellow/green), of nanoparticles in lysosomes with a value of 1 for full co-localization. Co-localization coefficient represents the relative level of nanoparticles in lysosomes (co-localized yellow pixels) as compared to the total lysosome area (overall sum of red pixels).

4. Conclusion

In conclusion, we have described the synthesis of water-soluble porphyrins for covalent encapsulation in silica-based nanoparticles with organized porosity. All the synthesized nanoparticles were efficient for PDT on breast cancer cells MDA-MB-231. The PDT efficiency of the nanoparticles was not only correlated with the quantum yield production of singlet oxygen but is rather determined by cellular uptake and subcellular localization of the nanoparticles in the organelles. The most efficient pathway consists of functionalizing the surface of the nanoparticles with α-mannose in order to get an active endocytosis of the nanoparticles by cancer cells. The quantity of mannose is critical and a too high density of carbohydrates on the surface of the nanoparticles impairs the penetration inside the cells. The nanoparticles are localized in the lysosomes after active endocytosis by mannose receptors. The data demonstrates that the optimization of the different parameters of these multifunctional nanoparticles is a relevant prerequisite before their *in vivo* PDT application.

Acknowledgements

Financial support by ANR PNANO. 07-102 and the non-profit organization Rétinostop is gratefully acknowledged. We thank Dr. C. Gérardin for DLS measurements and Mr. M. Gleizes for technical assistance in cell biology experiments. The authors wished to thank Ms. M. Bombled (URM 176 CNRS/Institut Curie, Institut Curie, Centre Universitaire, Orsay, France) for electrospray mass spectroscopy experiments and Mr. V. Guérineau (CNRS, ICSN, Gif sur Yvette, France) for MALDI-TOF analysis.

References

Ballut, S., Makky, A., Loock, B., Michel, J.P., Maillard, P., Rosilio, V., 2009. New strategy for targeting of photosensitizers. Synthesis of glycodendrimeric phenylporphyrins, incorporation into a liposome membrane and interaction with a specific lectin. Chem. Commun., 224–226.

Bechet, D., Couleaud, P., Frochot, C., Viriot, M.-L., Guillemin, F., Barberi-Heyob, M., 2008. Nanoparticles as vehicles for delivery of photodynamic therapy agents. Trends Biotechnol 26, 612–621.

Brevet, D., Gary-Bobo, M., Raehm, L., Richeter, S., Hocine, O., Amro, K., Loock, B., Couleaud, P., Frochot, C., Morere, A., Maillard, P., Garcia, M., Durand, J.O., 2009. Mannose-targeted mesoporous silica nanoparticles for photodynamic therapy. Chem. Commun., 1475–1477.

Chatterjee, D.K., Fong, L.S., Zhang, Y., 2008. Nanoparticles in photodynamic therapy: an emerging paradigm. Adv. Drug. Deliv. Rev. 60, 1627–1637.

Cheng, S.-H., Lee, C.-H., Chen, M.-C., Souris, J.S., Tseng, F.-G., Yang, C.-S., Mou, C.-Y., Chen, C.-T., Lo, L.-W., 2010. Tri-functionalization of mesoporous silica nanoparticles for comprehensive cancer theranostics—the trio of imaging, targeting and therapy. J. Mater. Chem. 20, 6149–6157.

Cheng, S.-H., Lee, C.-H., Yang, C.-S., Tseng, F.-G., Mou, C.-Y., Lo, L.-W., 2009. Mesoporous silica nanoparticles functionalized with an oxygen-sensing probe for cell photodynamic therapy: potential cancer theranostics. J. Mater. Chem. 19, 1252–1257.

Couleaud, P., Morosini, V., Frochot, C., Richeter, S., Raehm, L., Durand, J.O., 2010. Silica-based nanoparticles for photodynamic therapy applications. Nanoscale 2, 1083–1095.

Davydenko, M.O., Radchenko, E.O., Yashchuk, V.M., Dmitruk, I.M., Prylutskyy, Y.I., Matishevska, O.P., Golub, A.A., 2006. Sensibilization of fullerene c-60 immobilized at silica nanoparticles for cancer photodynamic therapy. J. Mol. Liq. 127, 145–147.

De la Fuente, J.M., Penades, S., 2006. Glyconanoparticles: types, synthesis and applications in glycoscience, biomedicine and material science. Biochem. Biophys. Acta 1760, 636–651.

DeRosa, M.C., Crutchley, R.J., 2002. Photosensitized singlet oxygen and its applications. Coord. Chem. Rev. 233, 351–371.

Derrien, G., Charnay, C., Zajac, J., Jones, D.J., Roziere, J., 2008. Copper-containing monodisperse mesoporous silica nanospheres by a smart one-step approach. Chem. Commun., 3118–3120.

Dick, D.L., Rao, T.V.S., Sukumaran, D., Lawrence, D.S., 1992. Molecular encapsulation—cyclodextrin-based analogs of heme-containing proteins. J. Am. Chem. Soc. 114, 2664–2669.

Gu, H., Xu, K., Yang, Z., Chang, C.K., Xu, B., 2005. Synthesis and cellular uptake of porphyrin decorated iron oxide nanoparticles-a potential candidate for bimodal anticancer therapy. Chem. Commun., 4270–4272.

Hao, E., Friso, E., Miotto, G., Jori, G., Soncin, M., Fabris, C., Sibrian-Vazquez, M., Vicente, M.G.H., 2008. Synthesis and biological investigations of tetrakis(p-carboranylthio-tetrafluorophenyl)chlorin (tpfc). Org. Biomol. Chem. 6, 3732–3740.

Hu, L., Mao, Z.W., Gao, C.Y., 2009. Colloidal particles for cellular uptake and delivery. J. Mater. Chem. 19, 3108–3115.

Huang, D.-M., Hung, Y., Ko, B.-S., Hsu, S.-C., Chen, W.-H., Chien, C.-L., Tsai, C.-P., Kuo, C.-T., Kang, J.-C., Yang, C.-S., Mou, C.-Y., Chen, Y.-C., 2005. Highly efficient cellular labeling of mesoporous nanoparticles in human mesenchymal stem cells: implication for stem cell tracking. FASEB J. 19, 2014–2016.

Huang, X.L., Teng, X., Chen, D., Tang, F.Q., He, J.Q., 2010. The effect of the shape of mesoporous silica nanoparticles on cellular uptake and cell function. Biomaterials 31, 438–448.

Koo, Y.E.L., Reddy, G.R., Bhojani, M., Schneider, R., Philbert, M.A., Rehemtulla, A., Ross, B.D., Kopelman, R., 2006. Brain cancer diagnosis and therapy with nanoplatforms. Adv. Drug. Deliv. Rev. 58, 1556–1577.

Kopelman, R., Koo, Y.E.L., Philbert, M., Moffat, B.A., Reddy, G.R., McConville, P., Hall, D.E., Chenevert, T.L., Bhojani, M.S., Buck, S.M., Rehemtulla, A., Ross, B.D., 2005. Multifunctional nanoparticle platforms for *in vivo* mri enhancement and photodynamic therapy of a rat brain cancer. J. Magn. Magn. Mater. 293, 404–410.

Lai, C.-W., Wang, Y.-H., Lai, C.-H., Yang, M.-J., Chen, C.-Y., Chou, P.-T., Chan, C.-S., Chi, Y., Chen, Y.-C., Hsiao, J.-K., 2008. Iridium-complex-functionalized Fe_3O_4/SiO_2 core/shell nanoparticles: a facile three-in-one system in magnetic resonance imaging, luminescence imaging, and photodynamic therapy. Small 4, 218–224.

Lebret, V., Raehm, L., Durand, J.O., Smaihi, M., Gerardin, C., Nerambourg, N., Werts, M.H.V., Blanchard-Desce, M., 2008. Synthesis and characterization of fluorescently doped mesoporous nanoparticles for two-photon excitation. Chem. Mater. 20, 2174–2183.

Lerouge, F., Melnyk, O., Durand, J.O., Raehm, L., Berthault, P., Huber, G., Desvaux, H., Constantinesco, A., Choquet, P., Detour, J., Smaihi, M., 2009. Towards thrombosis-targeted zeolite nanoparticles for laser-polarized xe-129 mri. J. Mater. Chem. 19, 379–386.

Lin, Y.-S., Tsai, C.-P., Huang, H.-Y., Kuo, C.-T., Hung, Y., Huang, D.-M., Chen, Y.-C., Mou, C.-Y., 2005. Well-ordered mesoporous silica nanoparticles as cell markers. Chem. Mater. 17, 4570–4573.

McCarthy, J.R., Jaffer, F.A., Weissleder, R., 2006. A macrophage-targeted theranostic nanoparticle for biomedical applications. Small 2, 983–987.

Mosmann, T., 1983. Rapid colorimetric assay for cellular growth and survival—application to proliferation and cyto-toxicity assays. J. Immunol. Methods 65, 55–63.

Ohulchanskyy, T.Y., Roy, I., Goswami, L.N., Chen, Y., Bergey, E.J., Pandey, R.K., Oseroff, A.R., Prasad, P.N., 2007. Organically modified silica nanoparticles with covalently incorporated photosensitizer for photodynamic therapy of cancer. Nano Lett. 7, 2835–2842.

Park, I.Y., Kim, I.Y., Yoo, M.K., Choi, Y.J., Cho, M.-H., Cho, C.S., 2008. Mannosylated polyethylenimine coupled mesoporous silica nanoparticles for receptor-mediated gene delivery. Int. J. Pharma. 359, 280–287.

Perrée-Fauvet, M., Verchère-Béaur, C., Tarnaud, E., Anneheim-Herbelin, G., Bône, N., Gaudemer, A., 1996. New amino acid porphyrin derivatives.1. Synth. Tetrahedron 52, 13569–13588.

Pinthus, J.H., Bogaards, A., Weersink, R., Wilson, B.C., Trachtenberg, J., 2006. Photodynamic therapy for urological malignancies: past to current approaches. J. Urol. 175, 1201–1207.

Reddy, G.R., Bhojani, M.S., McConville, P., Moody, J., Moffat, B.A., Hall, D.E., Kim, G., Koo, Y.E.L., Woolliscroft, M.J., Sugai, J.V., Johnson, T.D., Philbert, M.A., Kopelman, R., Rehemtulla, A., Ross, B.D., 2006. Vascular targeted nanoparticles for imaging and treatment of brain tumors. Clin. Cancer Res. 12, 6677–6686.

Ross, B., Rehemtulla, A., Ko, Y.E.L., Reddy, R., Kim, G., Behrend, C., Buck, S., Schneider, R.J., Philbert, M.A., Weissleder, R., Kopelman, R., 2004. Photonic and magnetic nanoexplorers for biomedical use: from subcellular imaging to cancer diagnostics and therapy. Nanobiophot. Biomed. Appl. 5331, 76–83.

Rossi, L.M., Silva, P.R., Vono, L.L.R., Fernandes, A.U., Tada, D.B., Baptista, M.S., 2008. Protoporphyrin ix nanoparticle carrier: preparation, optical properties, and singlet oxygen generation. Langmuir 24, 12534–12538.

Slowing, I., Trewyn, B.G., Lin, V.S.Y., 2006. Effect of surface functionalization of mcm-41-type mesoporous silica nanoparticles on the endocytosis by human cancer cells. J. Am. Chem. Soc. 128, 14792–14793.

Slowing, I.I., Wu, C.W., Vivero-Escoto, J.L., Lin, V.S.-Y., 2009. Mesoporous silica nanoparticles for reducing hemolytic activity towards mammalian red blood cells. Small 5, 57–62.

Sutton, J.M., Clarke, O.J., Fernandez, N., Boyle, R.W., 2002. Porphyrin, chlorin, and bacteriochlorin isothiocyanates: useful reagents for the synthesis of photoactive bioconjugates. Bioconjug. Chem. 13, 249–263.

Tu, H.-L., Lin, Y.-S., Hung, Y., Lo, L.-W., Chen, Y.-F., Mou, C.-Y., 2009. *In vitro* studies of functionalized mesoporous silica nanoparticles for photodynamic therapy. Adv. Mater. 21, 172–174.

Zhang, P., Steelant, W., Kumar, M., Scholfield, M., 2007. Versatile photosensitizers for photodynamic therapy at infrared excitation. J. Am. Chem. Soc. 129, 4526–4527.